Trans Indian Inst Met (2020) 73(9):2377–2386
https://doi.org/10.1007/s12666-020-02039-y

ORIGINAL ARTICLE

Phase Evolution and Thermal Stability of Low-Density MgAlSiCrFe High-Entropy Alloy Processed Through Mechanical Alloying

Nandini Singh[1] · Yagnesh Shadangi[1] · Nilay Krishna Mukhopadhyay[1]

Received: 30 January 2020 / Accepted: 8 July 2020 / Published online: 28 July 2020

Abstract An equiatomic MgAlSiCrFe high-entropy alloy was synthesized by mechanical alloying. The alloying behavior, phase evolution, phase composition and thermal stability of as-milled nanostructured powders of HEA were ascertained through X-ray diffraction and transmission electron microscopy, scanning electron microscopy and differential scanning calorimetry (DSC), respectively. The milling of elemental powders for 60 h led to the formation of HEA with a major BCC phase having lattice parameter of 0.2887 ± 0.005 nm very close to that of the α-Fe and a minor fraction of undissolved Si. The nanocrystalline HEA powder formed during milling has crystallite size of 19 ± 0.8 nm. The STEM–EDS mapping of these milled powders confirms the homogenous elemental distribution after 60 h of mechanical alloying. The DSC thermogram of 60 h milled HEA powder shows the thermal stability of milled powder up to ∼ 400 °C. The exothermic heating events observed in the DSC thermogram correspond to phase transformation of MgAlSiCrFe HEA powder, and it may be correlated with the phases observed through the ex situ XRD of HEA powders annealed at different temperatures up to 700 °C. After annealing the 60 h milled powder, various phases along with parent BCC phase have evolved, i.e., B2 type Al–Fe phase, FCC phases (Al–Mg solid solution), Cr_5Si_3, Mg_2Si, $Al_{13}Fe_4$. Further, the experimental findings were correlated with various thermodynamic parameters for understanding the phase evolution and stability.

✉ Nandini Singh
nandini.rs.met13@iitbhu.ac.in

[1] Department of Metallurgical Engineering, Indian Institute of Technology (BHU), Varanasi, Uttar Pradesh 221005, India

Keywords Low-density HEA · Mechanical alloying · Phase evolution · Thermal stability

1 Introduction

The upsurge in the demand for materials with high strength-to-weight ratio has led to design and development of many new classes of materials. The conventionally used alloys for engineering applications are mostly based on a single element with minor addition of other elements to enhance its mechanical and functional properties [1]. In the last three decades, considerable efforts were made by researchers toward development of high-strength materials. This led to the discovery of quasicrystals [2], bulk metallic glasses [3] and high-entropy alloys [4, 5]. Among the various new classes of materials developed, the high-entropy alloys (HEAs) are a relatively new category of alloys based on highly concentrated multicomponent elements. High-entropy alloys are defined as multicomponent alloys with five or more elements having a concentration between 5 and 35 at.% [6–10]. They can form a solid solution, intermetallics or bulk metallic glasses depending on composition and processing routes selected [9, 11, 12]. As per the recent review published on HEAs, Steurer has reported the existence of only 80 single-phase high-entropy alloys till date [13]. However, during the last decade, HEAs have become a part of immense research owing to their excellent structural properties like hardness, strength, ductility as well as functional properties like magnetic and electrical [1]. Most of the high-entropy alloys so far studied consist of transition elements like Cr, Fe, Co, Ni and non-transition elements with atomic size and electronegativity close to them [14–21]. Although the HEAs containing transition metals with or without addition of Al have high strength,

the density of such alloys is more than 7.0 g cm^{-3} [22–25]. A few of the recent literature on HEAs have described the concept of low-density high-entropy alloys (LDHEA), having density $\leq$ 5.0 g cm^{-3} [26–32]. However, there is very limited literature on low-density high-entropy alloys exhibiting less density compared to the transition metals based HEAs. There have been also very few studies on low-density high-entropy alloys (LDHEAs) comprising of non-transition metals elements like Mg and Si. Youssef et al. [27] showed the formation of complete FCC phase after 16 h of MA in $Al_{20}Li_{20}Mg_{20}Sc_{20}Ti_{20}$. Chen et al. [33] studied BeCoMgTi and BeCoMgTiZn HEAs synthesized by MA and demonstrated the amorphization of HCP elements. Kai et al. [34] developed $Al_{20}Be_{20}Fe_{20}Si_{20}Ti_{35}$ by casting route having density of 3.91 g cm^{-3}. There are several well-established existing methods for synthesis of HEAs, e.g., casting, but in the present investigation, we have chosen the mechanical alloying technique because it is a relatively easier method to synthesize alloys from the constituent elemental metal powders [35]. Also, unlike casting route, segregations and inhomogeneity of structure can be avoided in mechanical alloying route [1] and most of the cases lead to the formation of single solid solution phase.

In the present investigation, efforts were made to study the alloying behavior of low-density HEAs by incorporating elements like Mg and Si (having HCP and diamond cubic crystal structure respectively) with Al (FCC), Cr (BCC) and Fe (BCC) elements and processing through mechanical alloying route. The mechanical alloying is the most preferred technique for synthesis of MgAlSiCrFe HEA, as to negate the phase separation tendency arising from the positive enthalpy of mixing among the binary alloys. Further efforts were also made to establish the thermal stability of MgAlSiCrFe HEAs up to an elevated temperature of 700 °C. The effect of Mg and Si on possible solid solution formation has been discussed in accordance with the various thermodynamic and fundamental properties.

2 Experimental Details

The elemental powders of Mg, Al, Si, Cr and Fe (purity > 99%; powder particle size < 75 μm) having nominal composition of $Mg_{20}Al_{20}Si_{20}Cr_{20}Fe_{20}$ (at.%) were mechanically alloyed through high-energy ball milling. The mechanical alloying was carried out in a planetary ball mill (make: Retsch, Germany; model: PM 400/2) with a milling speed of 200 r.p.m. and ball-to-powder ratio of 10:1. The elemental powders were taken in a 250 ml tungsten carbide (WC) vials with 10 mm WC balls having toluene as a process control reagent. The milling was continued up to 60 h, and samples were drawn after every 10 h. The milling was intermittently stopped for 15 min after every 30 min of operation to avoid any excessive rise in the temperature during milling. The details of the milling operation and procedure are described elsewhere [36–39].

The phase evolution of MgAlSiCrFe HEA was ascertained through X-ray diffractometer [make: Rigaku, Japan; model: MiniFlex, 600 W Benchtop XRD; source: Cu-K_α (λ = 0.15402 nm)] operating at 40 kV/20 mA with a scanning speed of 10°/min. The morphology, microstructure and elemental distribution of milled powders were established through scanning electron microscope (make: FEI; model: Quanta 200F) operating at 30 kV and equipped with energy-dispersive X-ray spectroscopy (EDS) detector. The fine microstructural features and nanostructured nature of 60 h milled powder were discerned through transmission electron microscopy (make: FEI; model: TECNAI G^2T20) operating at 200 kV. Further, the STEM–EDS mapping of 60 h milled powder was used for observing the compositional homogeneity in the LDHEA sample.

The thermal stability of 60 h milled powders was evaluated through differential scanning calorimeter (make: NETZSCH, Germany; model: DSC 404F3 Pegasus) at a heating rate of 40 k/min up to 800 °C in a nitrogen atmosphere. The heating events observed through the DSC have been correlated with the phases observed in ex-situ XRD of annealed powders at elevated temperatures. The 60 h milled samples were vacuum sealed in a quartz tube back filled with argon gas. The milled samples were annealed from 400 to 700 °C with an interval of 100 °C. The samples were annealed with a heating rate of 5 °C/min and held at desired temperature for 60 min, followed by furnace cooling.

3 Results

Figure 1 shows the phase evolution during mechanical alloying of MgAlSiCrFe HEA powders milled up to 60 h. The diffraction peaks corresponding to all the alloying elements in MgAlSiCrFe HEA are observed in the mechanically milled powder for 1 h. The variation in the intensity of alloying elements may be attributed to difference in the atomic scattering factor of the elements. Continuous milling till 10 h leads to the disappearance of lower melting point elements, i.e., Mg and Al. Due to the 10 h milling, all the diffraction peaks of Mg disappear along with the minor peaks of Al still visible. The milling of these powders till 20 h lead to the complete disappearance of the diffraction peaks corresponding to that of Al. However, all the intese and weak diffraction peaks corresponding to Si are still evident. Further increasing the

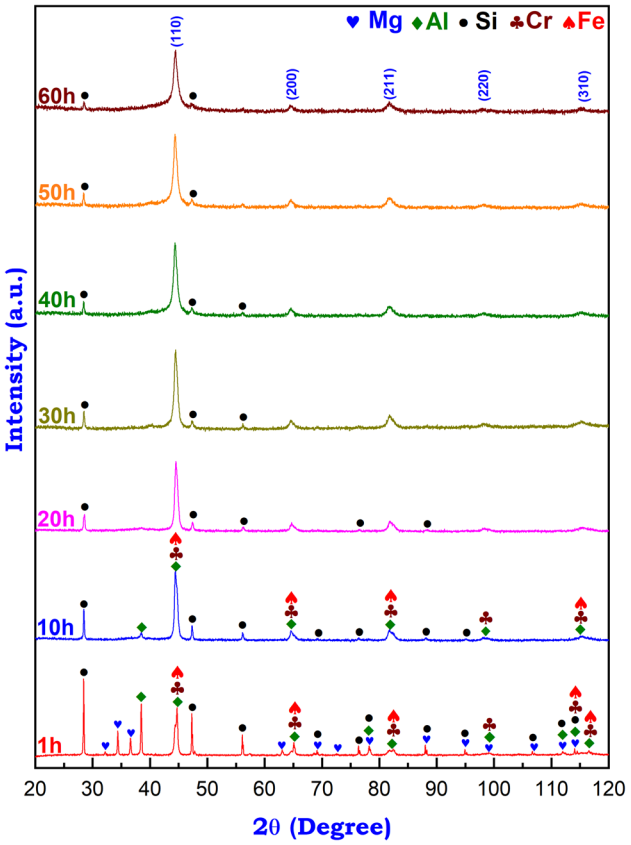

Fig. 1 Phase evolution during mechanical alloying of MgAlSiCrFe high-entropy alloy milled up to 60 h

milling duration up to 30 h leads to the formation of a major BCC phase solid solution with a minor phase fraction corresponding to that of the Si. (Only major reflection was observed). The major BCC phase in Fig. 1 shows all the intese reflections corresponding to that of the BCC, i.e., (110), (200), (211), (220) and (310). Although the major BCC type phase is observed as early as 30 h of milling without any asymmetric peak [associated with (110) peak of BCC phase], the milling is continued till 60 h for incorporation of minor fraction of retained Si into the solid solution. After 60 h of milling, the phase fraction of retained Si decreases as revealed from the reduced intensity of the reflections of Si i.e., (111), (220). It is observed that the milling induces significant broadening of the diffraction peaks corresponding to BCC type phase. The broadening of the peaks may be attributed to nanostructuring and lattice strain induced during milling up to 60 h. The crystallite size of 60 h mechanically alloyed powder is calculated by Williamson–Hall method [40]. The crystallite size of the MgAlSiCrFe HEA powder is $\sim 19 \pm 0.8$ nm, and it confirms the nanocrystalline nature of the mechanically alloyed MgAlSiCrFe high-entropy alloy powder. The precision lattice parameter of BCC phase is found to be 0.2887 ± 0.005 nm. Its value is found to be closer to BCC-Fe (0.2866 nm) which appears to act as a host lattice for other alloying elements.

The structure and fine microstructural features are identified through TEM micrographs shown in Fig. 2. The bright-field image, selected area diffraction pattern (SADP) and corresponding dark-field image of MgAlSiCrFe HEA

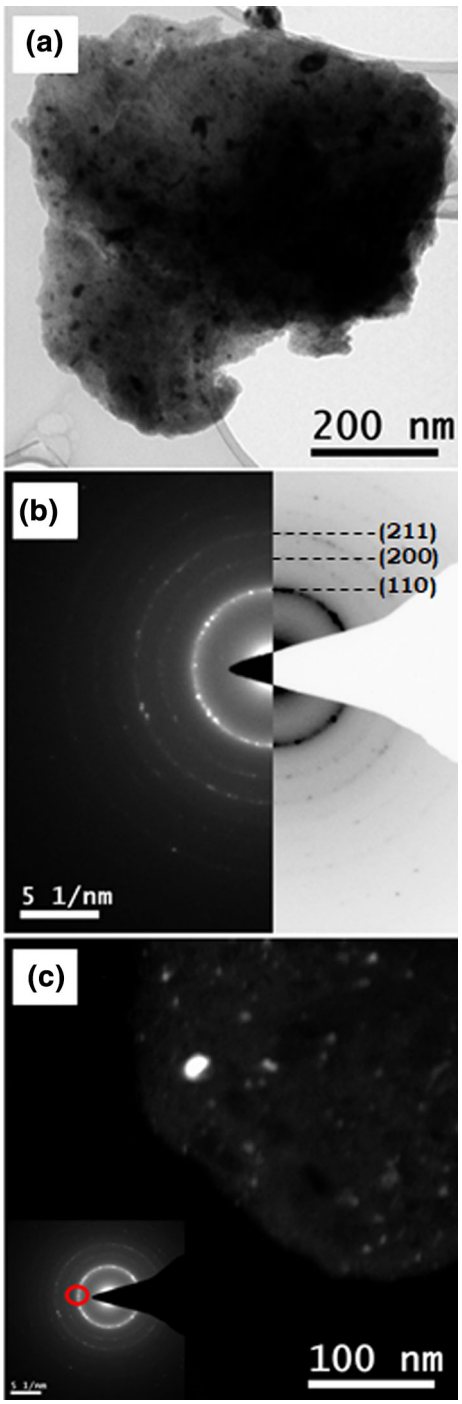

Fig. 2 TEM micrograph showing **a** bright-field image, **b** selected area diffraction pattern and **c** dark-field image of MgAlSiCrFe HEA powder milled for 60 h

powder are shown in Fig. 2a–c, respectively. The bright-field image (Fig. 2a) shows the presence of dark patches throughout the powder particle investigated. The nanostructured grains of ≤ 20 nm are also seen in the MgAlSiCrFe HEA powder particles. The dark patches observed in the bright-field images are due to the presence of strain accumulated during mechanical alloying for 60 h of the HEA powder particles. This observation is in line with the XRD pattern of 60 h milled HEA powder showing considerable broadening. The polycrystalline ring pattern shown in Fig. 2b have rings [i.e., (110), (200), (211)] corresponding to the BCC solid solution phase. However, the particle investigated does not show the minor fraction of retained Si. The polycrystalline nature of the SADP is due to the random orientation of the powder particles milled up to 60 h in a high-energy planetary ball mill. The nanocrystalline nature of the MgAlSiCrFe HEA powder is evident from Fig. 2c. The dark-field image corresponding to the (110) plane of the HEA powder shows the presence of nanostructured grains having a size of $\sim 15 \pm 4$ nm. The grain size observed through TEM investigation is very close to that of the crystallite size observed through XRD results shown in Fig. 1.

The elemental distribution of alloying elements in the MgAlSiCrFe HEA powder is studied through STEM–EDS elemental mapping. The STEM–EDS elemental mapping shows the homogenous distribution of all the alloying elements, i.e., Mg, Al, Si, Cr and Fe in HEA powder mechanically milled for 60 h. The absence of any signature of major heterogeneity confirms the incorporation of alloying elements into the BCC host lattice observed through XRD and TEM in Figs. 1 and 2, respectively. However, slight variation in the intensity of Cr may be discerned through the STEM–EDS map of MgAlSiCrFe HEA powder (Fig. 3). This may be attributed to the repeated fracturing and cold welding leading to the formation of HEA powder particles with variable size, shape and thickness. These parameters influence the interaction of the electron beam with the milled powder particles and the generation of X-ray signals leading to localized variation in the intensity during STEM–EDS mapping.

The SEM micrograph in Fig. 4a–c shows morphology of HEA powder particles mechanically alloyed for 20 h, 40 h and 60 h, respectively. It may be seen from Fig. 4 that milled particles are irregular in shape as well as size. From the BSE–SEM micrograph in Fig. 4a, two distinct type of color contrast may be observed, i.e., light gray and dark gray. However, on increasing the duration of milling, only light gray contrast may be observed (Fig. 4b, c) due to the homogenous distribution of elements and formation of a major single BCC phase solid solution already observed through XRD and TEM. The SEM micrograph of 60 h milled HEA powder also shows the presence of river-like pattern. This river-like pattern may be attributed to the cleavage fracture of powder particles due to repetitive fracturing and cold welding occurring during mechanical alloying/milling. The elemental composition of 60 h milled HEA powder particle is ascertained through SEM–EDS analysis and is reported in Table 1. The elemental composition obtained through SEM–EDS analysis is very close to that of the nominal chemical composition. This confirms the homogenous distribution of every elements at micrometer length scale.

The thermal stability of MgAlSiCrFe HEA powder has been established through differential scanning calorimetry by heating it up to 800 °C (1073 K) at scan rate of 40 K/min. The DSC thermogram shown in Fig. 5 represents four (04) exothermic heating events marked as T1, T2, T3 and T4 occurring at a temperature of 439 °C (712 K), 549 °C (822 K), 659 °C (932 K) and 734 °C (1007 K) respectively, and is seen to be stable up to 439 °C (712 K). The heating events correspond to the phase transformation taking place during heating of HEA powder particles. The phase evolution corresponding to the heating events can be ascertained through ex situ XRD of the annealed HEA powder treated up to 700 °C (973 K). Figure 6 shows the phase evolution during annealing of HEA powder particles at room temperature: 300 °C (573 K), 400 °C (673 K), 500 °C (773 K), 600 °C (873 K) and 700 °C (973 K). The 60 h milled powder particle at room temperature has a major BCC phase solid solution with a minor fraction of the retained Si. The MgAlSiCrFe HEA powder particle is thermally stable up to 300 °C (573 K) as discerned from Fig. 6a. There may be some difference in the results obtained for thermal stability for milled powder particles through non-isothermal heating in DSC and isothermal annealing treatment. There are no additional phases formed apart from diffraction peaks corresponding to a major BCC phase (parent phase) and minor Si phase. On annealing the powder at 400 °C (673 K) along with the parent phase and minor Si phase, additional peaks corresponding to the partially ordered B2-type AlFe phase (cP2; $a = b = c =$ 0.2889 nm; $\alpha = \beta = \gamma = 90°$) and Mg_2Si phase (cF12; $a = b = c = 0.6343$ nm; $\alpha = \beta = \gamma = 90°$) appear. On further annealing, the powder at 500 °C (773 K), minor fraction of Al–Mg solid solution phase (cF4; $a = b = c =$ 0.4082 nm; $\alpha = \beta = \gamma = 90°$) designated as FCC1 may be seen in addition to the phases observed and seen at 400 °C (673 K). The shallow exothermic heating event at T1 as shown in Fig. 5 may be attributed to the formation of FCC1 phase. The minor fraction of Si is evident only up to 500 °C (773 K); however, the (111) and (220) reflection of Si disappears after annealing the sample at 600 °C (873 K). At 600 °C (873 K), minor fraction corresponding to the $Al_{13}Fe_4$ phase (mC102; $a = 1.549$ nm, $b = 0.808$ nm, $c = 1.248$ nm; $\alpha = \beta = 90°$, $\gamma = 107.72°$) appears as

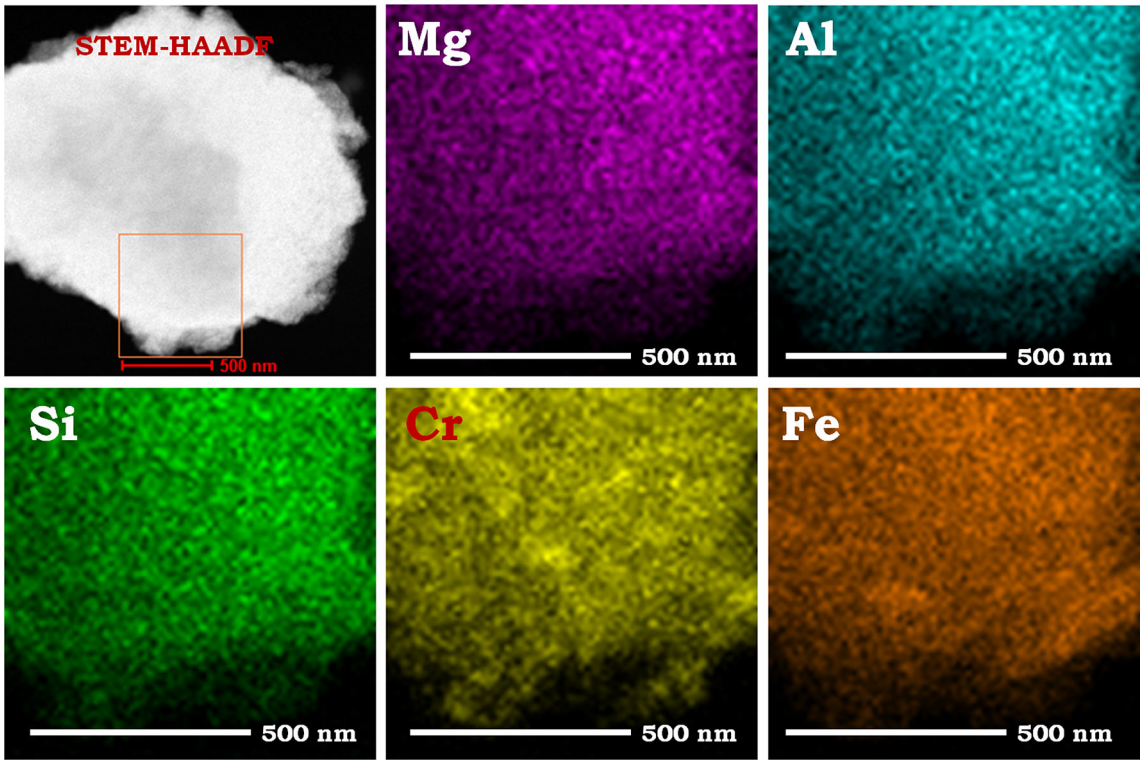

Fig. 3 STEM–EDS mapping of equiatomic MgAlSiCrFe high-entropy alloy mechanically alloyed for 60 h showing homogenous elemental distribution

observed in Fig. 6a, b along with parent BCC phase, B2-type AlFe phase, Mg_2Si phase and FCC1 phase. The exothermic heating event at T2 may be attributed to the formation of $Al_{13}Fe_4$ phase. On further increasing the annealing temperature to 700 °C (973 K), the FCC1 phase transforms to another Al–Mg solid solution phase (cF4; $a = b = c = 0.4215$ nm; $\alpha = \beta = \gamma = 90°$) designated as FCC2 having slightly different cell parameter from that of the FCC1 phase. Along with the parent phase, B2-type AlFe phase, $Al_{13}Fe_4$ phase, Mg_2Si phase, FCC2 phase and additional peaks corresponding to Cr_5Si_3 phase (tI32; $a = b$=0.917 nm, $c = 0.463$ Å; $\alpha = \beta = \gamma = 90°$) are also observed (Fig. 6). The exothermic heating event at T3 may be attributed due to transformation of FCC2 phase and formation of Cr_5Si_3 phase. Due to our experimental limitation, we are only able to systematically anneal the LDHEA powder up to 700 °C and study the phases evolved. However, the exothermic peak at T4 may be speculated to phase transformation of FCC2 (Al–Mg solid solution) phase to β-Al_3Mg_2 phase (cF1168; $a = b = c =$ 2.824 nm; $\alpha = \beta = \gamma = 90°$). The detailed analysis on high-temperature phase transformation of this LDHEA along with spark plasma sintering results will be published elsewhere.

4 Discussion

The phase evolution during mechanical alloying may be explained based on the various thermodynamic parameters related to MgAlSiCrFe high-entropy alloy. In order to explain the phase formation, three parameters namely enthalpy of mixing, the entropy of mixing and the atomic size difference have been calculated. The enthalpy of mixing of the five components MgAlSiCrFe HEA as calculated by regular solution model [41] has been found to be 15.84 kJ/mol. The enthalpy of mixing have been calculated by Miedema model for the proposed binary systems [42] and are mentioned in Table 2. The entropy of mixing by Boltzmann hypothesis formula mentioned in Yang et al. [41] was found to be 13.38 J/mol/k. The atomic size difference parameter 'δ' introduced by Yang and Zhang [41] was found to be around $\sim$ 12% (Table 3). According to prediction rule for the formation of solid solutions for multicomponent alloys, the proposed values of the enthalpy of mixing and the entropy of mixing should lie in the interval of $-$ 22 to 7 kJ/mol and 11 to 19.5 J/mol/k respectively. The atomic size difference should be $< 8.5\%$ [43]. Hence, the alloy system selected in our work is in good agreement with mixing enthalpy and mixing entropy. However, the deviation has been noticed in the third

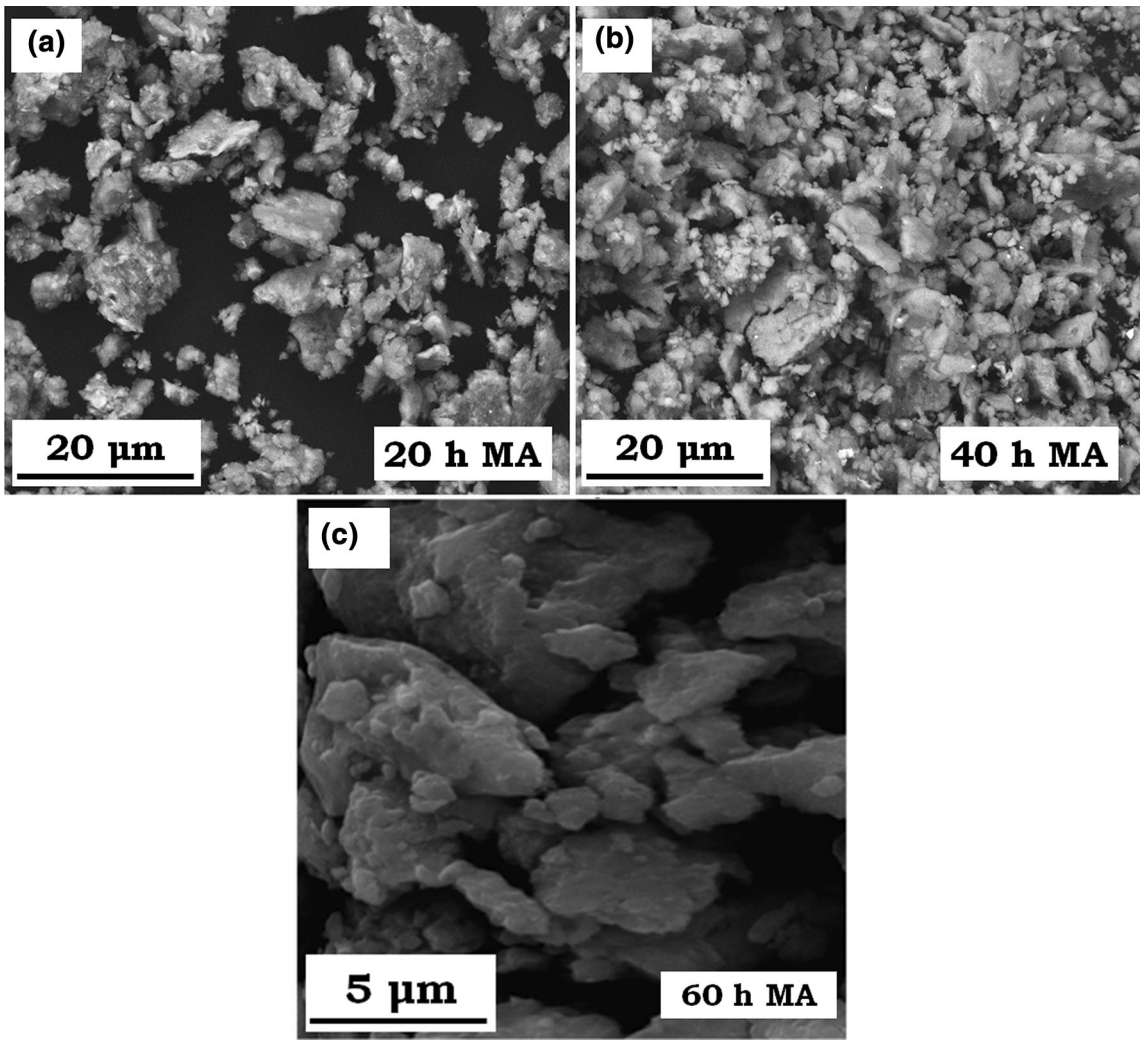

Fig. 4 SEM micrograph showing morphology and alloying of elements in MgAlSiCrFe HEA powder. **a** Mechanically alloyed for 20 h; **b** mechanically alloyed for 40 h and **c** mechanically alloyed for 60 h

Table 1 Elemental composition of MgAlSiCrFe HEA powder milled for 60 h

Sample designation of MgAlSiCrFe HEA powder	Milling duration (in h)	Elemental composition (at.%)				
		Mg	Al	Si	Cr	Fe
Desired composition	0	20	20	20	20	20
Final composition	60	20.39 ± 0.8	22.05 ± 1.2	19.20 ± 0.9	19.05 ± 1.0	19.28 ± 0.9

parameter i.e., atomic radius mismatch 'δ' which must be $< 8.5\%$. Yang and Zhang [41] proposed another parameter 'Ω' to predict the solid solution formation in HEAs. The valence electron concentration (VEC) was also described by Guo and Liu [43] to predict the structure. The Ω parameter and VEC have been calculated and found to be 3.18 and 4.6 respectively. They appear to be favourable for the formation of solid solution phases. The 'Ω' represents the ratio between the entropy and enthalpy of the system. The calculated thermodynamic parameter is mentioned in Table 3. MgAlSiCrFe HEA system having $\Omega > 1$ and VEC < 6.87 is in line with the criteria described for the formation of BCC phase.

The sequence of phase evolution during mechanical alloying of MgAlSiCrFe high-entropy alloy powder may be summarized as follows:

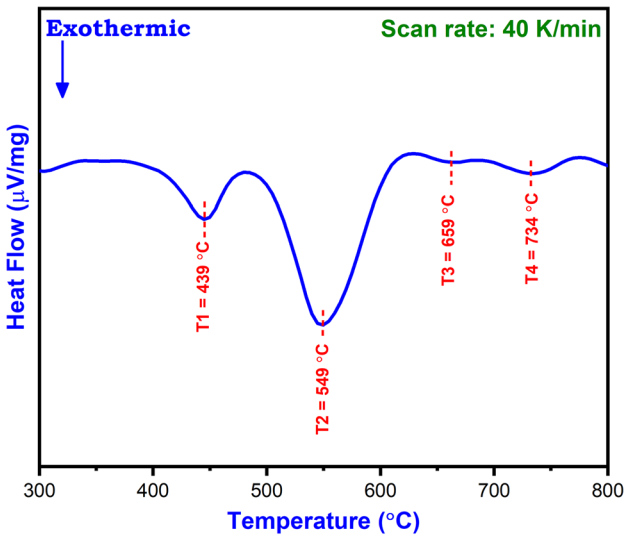

Fig. 5 DSC thermogram of MgAlSiCrFe HEA powder milled for 60 h showing exothermic heating events

Pre-mixed powders of Mg + Al + Si + Cr + Fe (0 h)	
1 h	→ Mg + Al + Si + Cr + Fe
10 h	→ Mg (disappear) + Al (minor peak disappears) + Si + Cr + Fe
20 h	→ Al (disappear) + Si + BCC phase + Cr ((110) asymmetric peak with BCC)
30 h	→ Si (minor peak disappear) + BCC phase
40 h	→ BCC phase (broadening) + Si (minor fraction)
50 h	→ BCC phase (broadening) + Si (minor fraction)
60 h	→ BCC phase (broadening) + Si (minor fraction; only (111) and (220) peaks remaining)

The disappearance of diffraction peaks can be seen as the beginning of solid solution formation. Chen et al. [44] showed the relationship between the alloying rate and melting point of alloying elements in HEA. The high melting point elements necessarily have higher bonding strength between the atoms. Peaks corresponding to high

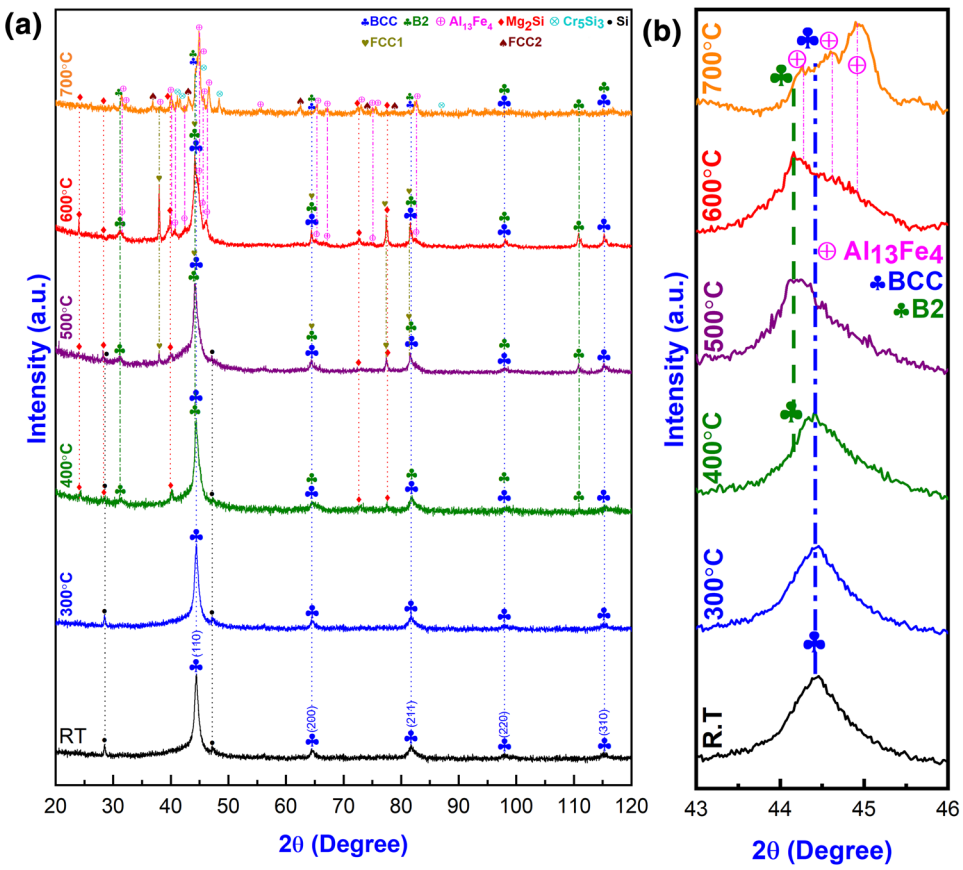

Fig. 6 **a** Phase evolution during annealing of 60-h milled MgAlSiCrFe HEA powder up to 700 °C (973 K) and **b** blown-up image for (110) peak of BCC phase showing evolution of other phases

m-

Table 2 Chemical enthalpy of mixing (ΔH_{ij}^{mix}, kJ/mol) of atomic pairs for MgAlSiCrFe high-entropy alloy, following the Miedema's approach

Elements	Mg	Al	Si	Cr	Fe
Mg	–	− 2	− 26	24	18
Al	− 2	–	− 2	− 10	− 11
Si	− 26	− 2	–	− 37	− 35
Cr	24	− 10	− 37	–	− 1
Fe	18	− 11	− 35	− 1	–

Table 3 Calculated thermodynamic and physical parameter of MgAlSiCrFe HEA

ΔH_{mix} (kJ/mol)	ΔS_{conf} (J K^{-1}/mol)	T_m (K)	Ω	δ (%)	VEC
− 15.84	13.38	1497	3.18	12	4.6

elting point elements i.e., Cr and Fe have maintained their identity; the lattice parameter suggests that Fe appears to be acting as host lattice to accommodate other alloying elements Mg, Al, Si and Cr.

Based on the experimental results, it is concluded that 60 h milling of MgAlSiCrFe HEA leads to the formation of a major BCC solid solution phase coexisting with minor amount of retained Si. The order in which the phases evolve mostly depends on the physical parameters of the constituent elements of equiatomic HEA given in Table 4. In principle melting point, atomic radii and self-diffusion coefficients are some of the decisive factors for sequence of phase evolution. Higher melting point elements have higher bond strength and stability in comparison with the elements with a low melting point and therefore, there is a probability of it to act as a host lattice for HEA. The self-diffusion coefficient also plays an important role in deciding the sequence of phase evolution. All the above factors dictate the sequence of phase evolution during the mechanical alloying of MgAlSiCrFe HEA. Cr has highest melting point among all the other elements used. Similarly, Mg possesses the highest self-diffusion coefficient and Si the lowest among all the elements used. Shivam et al. [14–16] have shown the role played by melting point of individual elements for their special affinity to form host lattice during the systematic investigation of phase evolution in AlCoCrFeMnNi, AlCoCrFeNi and AlCoCrFeNi-Ti HEA. The sequence is highly dependent on the bond strength of the elements used in the HEA. They have also reported the presence of minor phases of Mn along with the Fe and Cr as host lattice after completion of milling. Similar to the present case, Maulik et al. [45] have also shown the presence of two BCC phases with the increase in mole fraction of Mg in $Mg_XAlCrFeCu$ ($X = 1.0, 1.7$). Maulik et al. [45] have justified the sequence of phase evolution on the basis of bond strength and a function of melting point, atomic radii and self-diffusion coefficient. The sequence followed by the self-diffusion coefficient (D) is mentioned in Table 4. In spite of having lower melting point than Fe and Cr, Si is able to maintain its identity even after 60 h of MA due to its extremely lower diffusion coefficient, being one of the important parameters.

The MgAlSiCrFe HEA powder has been found to be thermally stable up to 439 °C (712 K). The sequence of phase evolution during annealing of the HEA is as follows:

Table 4 Physical parameter of constituent elements in MgAlSiCrFe HEA

Element	Mg	Al	Si	Cr	Fe
Atomic radius (Å)	1.62	1.438	1.18	1.249	1.241
Crystal structure	HCP	FCC	DC	BCC	BCC
Melting point (°C)	650	660	1410	1863	1538
Self-diffusion coefficient	10^{-13}	10^{-19}	10^{-62}	10^{-41}	10^{-31}

	Major phases	Minor phases
R.T →	BCC (Fe-based)	Si
300 °C →	BCC (Fe-based)	Si
400 °C →	BCC (Fe-based)	B2-AlFe + Mg_2Si + Si
500 °C →	BCC (Fe-based) + B2-AlFe	FCC1 + Mg_2Si + Si
600 °C →	BCC (Fe-based) + B2-AlFe	FCC1 + Mg_2Si + $Al_{13}Fe_4$
700 °C →	BCC (Fe-based) + B2-AlFe + $Al_{13}Fe_4$	FCC2 + Mg_2Si + Cr_5Si_3

Due to the negative enthalpy of mixing between binary elements such as Al–Fe (− 11 kJ/mol), Cr–Si (− 37 kJ/mol), Mg–Si (− 26 kJ/mol), Al–Mg (− 2 kJ/mol), the formation of compounds between these elements is thermodynamically more favorable. The large atomic size difference between elements lead to the solid solution plus intermetallic microstructure in annealed MgAlSiCrFe sample. Though milled MgAlSiCrFe HEA powder contains BCC phase along with some minor amount of undissolved Si, after annealing, some volume fraction of BCC phase is transformed to partially ordered BCC phase (B2 type) and other complex phases have also evolved. It is because, supersaturating solid solution of all the elements in the single BCC phase after mechanical alloying, lead to the formation of complex phase while annealing [44]. Maullik et al. [45, 46] have reported the thermal stability of Mg_XAlCrFeCu (X = 0, 0.5, 1.0, 1.7) up to 500 °C (773 K). They have further reported the formation of B2-type AlFe phase along with minor fraction corresponding to disordered BCC, Cu_2Mg, Mg_2Cu for Mg_XAlCrFeCu (X = 1.0, 1.7) phases in the spark plasma sintered [at 800 °C (1073 K)] sample. Similarly, in an investigation, Li et al. [47] have reported the formation of a major HCP-based phase along with the formation of minor fraction corresponding to Al–Mn icosahedral quasicrystalline phase in $Mg_x(MnAlZnCu)_{100-x}$ (X = 20, 33, 43, 45.6, 50 at.%) HEAs. They have further reported their stability up to 600 °C (873 K). In the present investigation also, major phases pertaining to B2-type AlFe, disordered BCC and $Al_{13}Fe_4$ phase are observed. Our understanding on the phase evolution and thermal stability of MgAlSiCrFe low-density HEA will definitely help toward the design and development of lightweight material for transportation industry.

5 Conclusions

In the present work, efforts were made to study the alloying behavior and thermal stability of MgAlSiCrFe low-density high-entropy alloy through mechanical alloying. The following conclusions can be drawn:

- A nanocrystalline equiatomic MgAlSiCrFe high-entropy alloy having a major solid solution phase coexisting with minor amount of undissolved Si was synthesized after mechanical alloying for 60 h. The disordered BCC phase solid solution having a lattice parameter close to that of α-Fe (a = 0.2887 ± 0.005 nm) was confirmed. The minor fraction of retained Si could not be dissolved completely like other elements into BCC phase even after 60 h of milling.
- The nanocrystalline nature of 60 h milled MgAlSiCrFe LDHEA powder was corroborated through TEM confirming the formation of BCC phase having a size of ∼ 19 nm. The STEM–EDS mapping establishes the homogenous distribution of alloying elements in the milled powder particles.
- The 60 h milled LDHEA powder was found to be thermally stable up to a temperature of 400 °C. The phase transformation above 400 °C has been observed. At 700 °C, the annealing treatment has led to the formation of a major BCC phase and B2-type AlFe phase with a few minor phases, i.e., FCC phases (Al–Mg solid solution), Cr_5Si_3, Mg_2Si, $Al_{13}Fe_4$.
- The ratio of – TΔS/ΔH is ∼ 3.2, which is in the range of solid solution forming HEAs as reported in the literature. The VEC value of 4.6 for this alloy indicates the possibility of formation of a single BCC phase. While deviation of atomic size mismatch factor (∼ 12%) may be held responsible for giving rise to a variety of phases after annealing treatment of milled alloyed powder of a nearly single solid solution phase. The high positive enthalpy of mixing among binary Mg–Cr, Mg–Fe and high negative enthalpy of mixing among Mg–Si, Cr–Si, Fe–Si are also not favorable for the formation of a single-phase high-entropy solid solution. Thus, the selection of alloying elements is of paramount importance for developing single-phase solid solution in a multicomponent system.

Acknowledgements Authors would like to thank Profs. B.N. Sarma, Sandip Chatterjee, K.G. Prashanth, and Dr. Joysurya Basu and Mr. Vikas Shivam for stimulating discussion. Authors would also like to acknowledge the support of Central Instrument Facility, IIT (BHU), and Dr Rampada Manna, Coordinator, Advanced Research Centre for Iron and Steel for extending necessary characterization facility. Authors wish to thank the Department of Science and Technology (DST) for infrastructural support under the scheme "Funds for

Improvement of S&T Infrastructure (FIST)" Level-II. Authors thankfully acknowledges technical help of Mr. Lalit Kumar Singh and Girish Sahoo for TEM and SEM investigations.

References

1. Murty B S, Yeh J W, and Ranganathan S, *High-Entropy Alloys*, 1st edition, Elseveir Inc, New York (2014).
2. Shechtman D, Blech I, Gratias D, and Cahn J W, *Phys Rev Lett* **53** (1984) 1951.
3. Inoue A, *Acta Mater* **48** (2000) 279. https://doi.org/10.1016/S1359-6454(99)00300-6.
4. Cantor B, Chang I T H, Knight P, and Vincent A J B, *Mater Sci Eng A* **375–377** (2004) 213. https://doi.org/10.1016/j.msea.2003.10.257.
5. Yeh J W, Chen S K, Lin S J, Gan J Y, Chin T S, Shun T T, Tsau C H, and Chang S Y, *Adv Eng Mater* **6** (2004) 299. https://doi.org/10.1002/adem.200300567.
6. Mukhopadhyay N K, *Curr Sci* **109** (2015) 665. http://www.jstor.org/stable/24905720.
7. Gao M C, *JOM* **67** (2015) 2251. https://doi.org/10.1007/s11837-015-1609-z.
8. Miracle D B, *Mater Sci Technol* **31** (2015) 1142. https://doi.org/10.1179/1743284714Y.0000000749.
9. Miracle D B, and Senkov O N, *Acta Mater* **122** (2017) 448. https://doi.org/10.1016/j.actamat.2016.08.081.
10. Miracle D B, *Nat Commun* **10** (2019) 1. https://doi.org/10.1038/s41467-019-09700-1.
11. Senkov O N, and Miracle D B, *J Alloys Compd* **658** (2016) 603. https://doi.org/10.1016/j.jallcom.2015.10.279.
12. Gorsse S, Miracle D B, and Senkov O N, *Acta Mater* **135** (2017) 177. https://doi.org/10.1016/j.actamat.2017.06.027.
13. Steurer W, *Mater Charact* (2020) 124658. https://doi.org/10.1016/j.colsurfa.2020.124658.
14. Shivam V, Basu J, Shadangi Y, Singh M K, and Mukhopadhyay N K, *J Alloys Compd* **757** (2018). https://doi.org/10.1016/j.jallcom.2018.05.057.
15. Shivam V, Basu J, Pandey V K, Shadangi Y, and Mukhopadhyay N K, *Adv Powder Technol* **29** (2018). https://doi.org/10.1016/j.apt.2018.06.006.
16. Shivam V, Shadangi Y, Basu J, and Mukhopadhyay N K, *J Mater Res* **34** (2019) 787. https://doi.org/10.1557/jmr.2019.5.
17. Yadav T P, Mukhopadhyay S, Mishra S S, Mukhopadhyay N K, and Srivastava O N, *Philos Mag Lett* **0839** (2018) 1. https://doi.org/10.1080/09500839.2017.1418539.
18. Mohanty S, Gurao N P, Padaikathan P, and Biswas K, *Mater Charact* **129** (2017) 127.
19. Mohanty S, Gurao N P, and Biswas K, *Mater Sci Eng A* **617** (2014) 211. https://doi.org/10.1016/j.msea.2014.08.046.
20. Shivam V, Sanjana V, and Mukhopadhyay N K, *Trans Indian Inst Met* **73** (2020) 821. https://doi.org/10.1007/s12666-020-01892-1.
21. Jain H, Shadangi Y, Shivam V, Chakravarty D, Kumar D, Shadangi Y, Shivam V, Chakravarty D, Mukhopadhyay N K, and Kumar D, *J. Pre-Proof* (2020).
22. Wang Z, Wu M, Cai Z, Chen S, and Baker I, *Intermetallics* **75** (2016) 79. https://doi.org/10.1016/j.intermet.2016.06.001.
23. Shaysultanov D G, Salishchev G A, Ivanisenko Y V, Zherebtsov S V, Tikhonovsky M A, and Stepanov N D, *J Alloys Compd* **705** (2017) 756. https://doi.org/10.1016/j.jallcom.2017.02.211.
24. Stepanov N D, Shaysultanov D G, Yurchenko N Y, Zherebtsov S V, Ladygin A N, Salishchev G A, and Tikhonovsky M A, *Mater Sci Eng A* **636** (2015) 188. https://doi.org/10.1016/j.msea.2015.03.097.
25. Deng Y, Tasan C C, Pradeep K G, Springer H, Kostka A, and Raabe A, *Acta Mater* **94** (2015) 124. https://doi.org/10.1016/j.actamat.2015.04.014.
26. Qiu Y, Hu Y J, Taylor A, Styles M J, Marceau R K W, Ceguerra A V, Gibson M A, Liu Z K, Fraser H L, and Birbilis N, *Acta Mater* **123** (2017) 115. https://doi.org/10.1016/j.actamat.2016.10.037.
27. Youssef K M, Zaddach A J, Niu C, Irving D L, and Koch C C, *Mater Res Lett* **3** (2014) 95. https://doi.org/10.1080/21663831.2014.985855.
28. Hammond V H, Atwater M A, Darling K A, Nguyen H Q, and Kecskes L J, *JOM* **66** (2014) 2021. https://doi.org/10.1007/s11837-014-1113-x.
29. Yang X, Chen S Y, Cotton J D, and Zhang Y, *JOM* **66** (2014) 2009. https://doi.org/10.1007/s11837-014-1059-z.
30. Sanchez J M, Vicario I, Albizuri J, Guraya T, and Garcia J C, *J Mater Res Technol* **8** (2019) 795. https://doi.org/10.1016/j.jmrt.2018.06.010.
31. Feng R, Gao M C, Zhang C, Guo W, Poplawsky J D, Zhang F, Hawk J A, Neuefeind J C, Ren Y, and Liaw P K, *Acta Mater* **146** (2018) 280. https://doi.org/10.1016/j.actamat.2017.12.061.
32. Raabe D, Tasan C C, Springer H, and Bausch M, *Steel Res Int* **86** (2015) 1127. https://doi.org/10.1002/srin.201500133.
33. Chen Y L, Tsai C W, Juan C C, Chuang M H, Yeh J W, Chin T S, and Chen S K, *J Alloys Compd* **506** (2010) 210. https://doi.org/10.1016/j.jallcom.2010.06.179.
34. Kokai T, Yachu Y, Chienchang J, Tsungshune C, Chewei T, and Jienwei Y E H, *Technol Sci* **61** (2018) 184.
35. Murty B S, and Ranganathan S, *Int Mater Rev* **43** (1998) 101. https://doi.org/10.1179/095066098790105654.
36. Shadangi Y, Shivam V, Singh M K, Chattopadhyay K, Basu J, and Mukhopadhyay N K, *J Alloys Compd* **797** (2019) 1280. https://doi.org/10.1016/J.JALLCOM.2019.05.128.
37. Shadangi Y, Sharma S, Shivam V, Basu J, Chattopadhyay K, Majumdar B, and Mukhopadhyay N K, *J Alloys Compd* (2020) 154258. https://doi.org/10.1016/J.JALLCOM.2020.154258.
38. Shadangi Y, Shivam V, Varalakshmi S, Basu J, Majumdar B, Mukhopadhyay N K, Shivam V, Varalakshmi S, Basu J, Chattopadhyay K, and Mukhopadhyay N K, *J. Pre-Proof* (2020).
39. Basariya M R, Roy R K, Pramanick A K, Srivastava V C, and Mukhopadhyay N K, *Mater Sci Eng A* **638** (2015) 282. https://doi.org/10.1016/j.msea.2015.04.076.
40. Williamson G K, and Hall W H, *Acta Metall* **1** (1953) 22. https://doi.org/10.1016/0001-6160(53)90006-6.
41. Yang X, and Zhang Y, *Mater Chem Phys* (2012). https://doi.org/10.1016/j.matchemphys.2011.11.021.
42. Miedema A R, de Châtel P F, and de Boer F R, *Phys B + C* **100** (1980) 1. https://doi.org/10.1016/0378-4363(80)90054-6.
43. Guo S C T L, *Prog Nat Sci Mater Int* **21** (2011) 433.
44. Chen Y L, Hu Y H, Hsieh C A, Yeh J W, and Chen S K, *J Alloys Compd* **481** (2009) 768. https://doi.org/10.1016/j.jallcom.2009.03.087.
45. Maulik O, Kumar D, Kumar S, Fabijanic D M, and Kumar V, *Intermetallics* **77** (2016) 46. https://doi.org/10.1016/j.intermet.2016.07.001.
46. Maulik O, and Kumar V, *Mater Charact* **110** (2015) 116. https://doi.org/10.1016/j.matchar.2015.10.025.
47. Li R, Gao J-C, and Fan K, *Mater Sci Forum* **686** (2011) 235. https://doi.org/10.4028/www.scientific.net/MSF.686.235.